Using ship-borne observations of methane isotopic ratio in the Arctic Ocean to understand methane sources in the Arctic

Berchet Antoine[1,*], Isabelle Pison[1], Patrick M. Crill[2], Brett Thornton[2], Philippe Bousquet[1], Thibaud Thonat[1], Thomas Hocking[1], Joël Thanwerdas[1], Jean-Daniel Paris[1] and Marielle Saunois[1]

[1]Laboratoire des Sciences du Climat et de l'Environnement, CEA-CNRS-UVSQ, IPSL, Gif-sur-Yvette, France.
[2]Department of Geological Sciences, Stockholm University, SE-10691 Stockholm, Sweden.

Correspondence: A. Berchet (antoine.berchet@lsce.ipsl.fr)

Abstract.

Due to the large variety and heterogeneity of sources in remote areas hard to document, the Arctic regional methane budget remain very uncertain. In situ campaigns provide valuable data sets to reduce these uncertainties. Here we analyse data from the SWERUS-C3 campaign, on-board the icebreaker *Oden*, that took place during summer 2014 in the Arctic Ocean along the

5 Northern Siberian and Alaskan shores. Total concentrations of methane, as well as isotopic ratios were measured continuously during this campaign for 35 days in July and August 2014. Using a chemistry-transport model, we link observed concentrations and isotopic ratios to regional emissions and hemispheric transport structures. A simple inversion system helped constraining source signatures from wetlands in Siberia and Alaska and oceanic sources, as well as the isotopic composition of lower stratosphere air masses. The variation in the signature of low stratosphere air masses, due to strongly fractionating chemical

10 reactions in the stratosphere, was suggested to explain a large share of the observed variability in isotopic ratios. These points at required efforts to better simulate large scale transport and chemistry patterns to use isotopic data in remote areas. It is found that constant and homogeneous source signatures for each type of emission in the region (mostly wetlands and oil and gas industry) is not compatible with the strong synoptic isotopic signal observed in the Arctic. A regional gradient in source signatures is highlighted between Siberian and Alaskan wetlands, the later ones having a lighter signatures than the first ones.

15 Arctic continental shelf sources are suggested to be a mixture of methane from a dominant thermogenic origin and a secondary biogenic one, consistent with previous in-situ isotopic analysis of seepage along the Siberian shores.

1   Introduction

Methane (CH_4) is both a potent greenhouse gas and a precursor of ozone with very diverse sources and sinks in the atmosphere (Saunois et al., 2016). About 60% (in mass) of CH_4 emissions to the atmosphere are due to microbial activity in anaerobic envi-

20 ronments: mainly natural wetlands, managed wetlands (such as rice paddies), landfills, waste-water facilities and the intestines of ruminants (domestic and wild) and termites. CH_4 is also emitted through fossil fuel leakages during extraction, transport and distribution. Finally, CH_4 is emitted by biomass burning (wildfires, agricultural fires and biofuels). The variety of CH_4 sources and their spatial and temporal heterogeneity make the uncertainties on CH_4 budgets very large, from the regional to the global

scales (Saunois et al., 2016). They impair our understanding of the variations of atmospheric concentrations, particularly of which sources and/or regions are causing these variations, which have been fast in the last decades (Dlugokencky et al., 2009; Nisbet et al., 2016; Saunois et al., 2017; Nisbet et al., 2019; Turner et al., 2019).

In the Arctic, major CH_4 sources are natural wetlands, in-land waters (lakes, streams, deltas, estuaries), leaks from oil and
5 gas extraction and transport, wildfires, seabed and geological seepage. The magnitude of all these sources suffers with very high uncertainties (McGuire et al., 2009; Kirschke et al., 2013; Arora et al., 2015; Berchet et al., 2016). The large areas of wetlands above 50°N and the high sensitivity of their CH_4 emissions to the changing climate make this zone a key-region for the global CH_4 budget. The present uncertainties on CH_4 sources and sinks in the Arctic are very large, due to the complexity of the involved processes and the difficult access to these remote regions (e.g., Thornton et al., 2016b; Bohn et al., 2015). Moreover,
10 in addition to increased CH_4 emissions from wetlands and thawing permafrost, increasing ocean temperatures could lead to the destabilization of methane clathrates on the Arctic continental shelf, potentially emitting large quantities of CH_4 , though there is no proof that such methane hydrate emissions are currently reaching the atmosphere in large quantities (Ruppel and Kessler, 2017). Other potential Arctic seafloor sources of CH_4 include emissions from degrading subsea permafrost (Dmitrenko et al., 2011), leakage from natural gas reservoirs, and degrading terrestrial organic carbon transported onto the continental shelf
15 (Charkin et al., 2011). CH_4 emissions from the Arctic would then have a positive feedback on climate change. Yet, The potential magnitude and timing of future methane emissions from the Arctic remain unsatisfactorily constrained. A better knowledge of Arctic CH_4 emissions would reduce uncertainties in its global budget, and help to better quantify the sensitivity of Arctic regional sources and sinks to climate change.

The current generation of satellites observing CH_4 with passive methods in the Short-Wave-InfraRed (SWIR) proves helpless
20 in providing a good coverage of Arctic regions, due to cloud, ice and snow cover, as well as the Arctic night (Xiong et al., 2008). The Merlin mission equipped with an active LIDAR is to be launched in 2024 and may radically improve the data coverage of CH_4 in the Arctic. For the time being and the next years, the monitoring of the Arctic atmosphere relies on in situ measurements. For more than ten years, atmospheric measurements of methane concentrations have been performed in the Arctic, either at surface stations (e.g., Arshinov et al., 2009; Sasakawa et al., 2010; Dlugokencky et al., 2014), during mobile field campaigns
25 such as the YAK-AEROSIB aircraft campaigns (Paris et al., 2010) or during oceanographic campaigns. In the present work, we analyze data from the SWERUS-C3 campaign on-board a ship in the Arctic Ocean during summer 2014 (Thornton et al., 2016a). Such short-term mobile campaigns are necessary to complement the limited number of long-term fixed, mostly coastal stations currently available. In particular, oceanic campaigns are expected to provide information on oceanic sources but also on land sources located upwind. However, CH_4 from various sources is being mixed during the atmospheric transport of the
30 air masses, which makes it difficult to separate them without resorting to numerical modelling (Berchet et al., 2016).

Atmospheric inversions merge together observations, numerical modelling and emission data sets to attribute the observed variability in CH_4 concentrations to emitting regions and thus optimize the CH_4 budget. Such methods were successfully applied in the Arctic using in situ fixed stations (e.g., Berchet et al., 2014; Thompson et al., 2017). But despite technical progress in numerical modelling and inversion methods, it is hardly feasible to separate co-located emissions from different
35 emitting sectors upwind observation sites based on CH_4 observations only. Observations of methane isotopic ratios could

help separating emission sectors as the main emission processes are isotopically fractionating, causing significantly different isotopic source signatures. For example, high-latitude wetlands were attributed signatures in a range of $-80/-55$‰ (Thornton et al., 2016b; Fisher et al., 2017; Ganesan et al., 2018). The δ^{13}C-CH$_4$ signature of atmospheric CH$_4$ above the Arctic Ocean has been previously reported in the range of $-50/-47$‰ (Yu et al., 2015; Pankratova et al., 2019). Isotopes have already been

5   used to characterise the origin of air masses in the Arctic (Fisher et al., 2011; Warwick et al., 2016) and these studies concluded that refinements in qualifying source emission isotopic signatures are required. In particular, in situ measurements of source signatures are being made in various environments but their strong variabilities make any upscaling difficult, pointing at the necessity of integrated information on emission signatures.

In the following, we explore the potential of using observations of isotopic ratios in the Arctic Ocean together with total

10   CH$_4$ concentrations to separate emission sources around the Arctic Circle. We further analyse emission isotopic signatures in the Arctic from integrated atmospheric observations. We base our analysis on the unique observation set collected during the ship-based campaign SWERUS-C3 during summer 2014 in the Arctic Ocean. By comparing measurements to simulations of total CH$_4$ and isotopic ratio, we analyse to what extent the observable signal in the Arctic Ocean is exploitable in a numerical inversion system. In Sect. 2, we explain our inversion approach alongside giving details on the SWERUS-C3 observation

15   campaign and on the model CHIMERE used in our study. In Sect. 3, we compare observations to simulations to assess the main contributions to the signal variability, and then implement a simplified inversion system to quantify isotopic emission signatures from various emission sectors around the Arctic

2   Methods

2.1   Campaign and instrument description

20   Observations were carried out during the SWERUS-C3 campaign onboard the Swedish icebreaker *Oden* between July 14th and September 26th, 2014. The cruise path was thru the central and outer Laptev and East Siberian seas, and finally the Chukchi Sea to Point Barrow, Alaska, in a first leg (see Fig. 1). A second leg of the cruise headed north from Point Barrow back through the Chukchi Sea and into the Arctic Ocean; atmospheric CH$_4$ observations continued until September 26th. As shown in Fig. S1 in supplementary materials, sea ice cover was present during a large portion of the campaign. Regions known to have active

25   seafloor gas seeps occurred in both ice-free (in the Laptev Sea) and ice-covered (in the East Siberian Sea) regions.

Concentrations of total CH$_4$ were measured during the whole campaign using an off-axis cavity ring-down laser spectrometer, from Los Gatos Research (LGR) Inc. (Model 0010, FGGA 24EP, Mountain View, California, USA). Air inlets were located at 9, 15, 20, and 35 m above the sea surface; air was pulled through all inlets continuously, and analyzed from one inlet at a time for 2 minutes before switching to the next inlet. Data was filtered using wind speed and direction to avoid contamination

30   from the ship exhaust. The spectrometer was calibrated every two hours using a two synthetic air target gases; the target gases themselves were calibrated before, during, and after the cruise to a NOAA Earth System Research Laboratory certified standard for CH$_4$. The reported precision was 0.5 ppb. Further details are available in Thornton et al. (2016a).
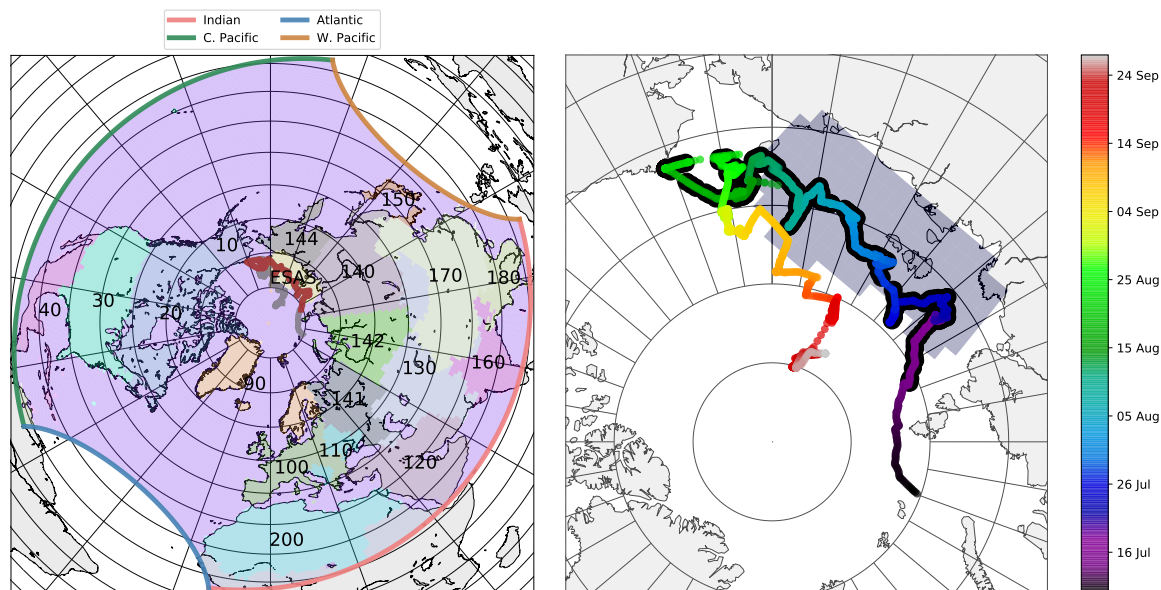
Figure 1. Path of the icebreaker *Oden* during the SWERUS-C3 campaign and domain of simulations. (left) The ship positions are represented by gray and brown dots, with brown points corresponding to locations where isotopic observations where carried out. The area delimited by coloured lines is the domain of CHIMERE simulations used for this study (see Sect. 2.2). The shaded areas and associated numbers correspond to the regions and their IDs used to separate contributions from remote emissions to the observed signal, as detailed in Sect. 2.3. ESAS = East Siberian Arctic Shelf. CHIMERE boundary conditions are split along the four sides of the domain as indicated by the coloured lines. (right) Zoom on the area covered by the campaign. The icebreaker's locations are coloured depending on their corresponding dates. Ship positions with a black edge are locations where isotopic observations where carried out. More details on the campaign in Thornton et al. (2016a). The shaded area corresponds to the ESAS emission region used in our simulation set up.

Isotopic ratios were measured only during the first leg of the campaign, from July 14th to August 26th (see Fig. 1) using an Aerodyne Research, Inc (Billerica, MA, USA) direct absorption interband cascade laser spectrometer. This spectrometer measured the concentrations of the CH_4 isotopologues $^{12}CH_4$, $^{13}CH_4$, and CH_3D, the latter of which is not discussed in the current paper. The more common isotope ratio mass spectrometry methods directly provide (as their name implies) an isotope ratio. In contrast, because the Aerodyne spectrometer measures the individual isotopologues, they must be individually calibrated before converting to δ^{13}C-CH_4 values; this method is described in McCalley et al. (2014).

2.2 Model description

The Eulerian model CHIMERE (Menut et al., 2013) was run to simulate total concentrations of CH_4 as well as partial $^{12}CH_4$ and $^{13}CH_4$ concentrations to compute CH_4 isotopic ratios afterwards using the following formula:

$$\delta^{13}C = \frac{\left(\frac{[^{13}C]}{[^{12}C]}\right)_{sim}}{\left(\frac{[^{13}C]}{[^{12}C]}\right)_{ref}} - 1 \qquad (1)$$

with $\left(\frac{[^{13}C]}{[^{12}C]}\right)_{ref} = 0.0112372$ the reference ratio from Craig (1957).

The domain of simulations spans over most of the North hemisphere with a horizontal resolution of $\sim 100\,km$ in order to include most contributions from distant sources (see Fig. 1). Similarly, the model uses 34 vertical levels from the surface up to $150\,hPa$ to represent stratosphere-to-troposphere intrusions. A spin-up period of six months prior to the campaign was used to properly assess the impact of air masses transported for long periods before reaching the Arctic ocean. The chemical sink of CH_4 by OH radicals is explicitly computed in CHIMERE using pre-computed fixed OH fields from the chemical model LMDZ-INCA.

CHIMERE runs use the following input data streams: (i) meteorological fields were downloaded from the European Centre for Medium Range Weather Forecasts (www.ecmwf.int) at $0.5°$ resolution every 3 hours; (ii) anthropogenic emissions were aggregated at the CHIMERE resolution from the EDGARv4.3.2 database at $0.1°$ horizontal resolution (Crippa et al., 2016); (iii) wetland emissions were interpolated from the model ORCHIDEE at $0.5°$ horizontal resolution (Ringeval et al., 2010); (iv) boundary CH_4 concentration fields were extracted from the general circulation model LMDZ; (v) and isotopic signatures of the different sources were chosen from Sherwood et al. (2017).

2.3 Atmospheric inversion of isotopic signature

Usually observations of $\delta^{13}C$-CH_4 are used to help constraining methane fluxes and differentiating between different sources with known signatures. However, the intrinsic spatial and temporal variability of source isotopic signatures limits the robustness of this approach (e.g., Fisher et al., 2017, as illustrated in Sect. 3.1). Here, we conversely assume that total CH_4 is properly simulated by our model (as confirmed by the good performance of the model to reproduce total CH_4 concentrations, highlighted in Sect. 3.1) and that the relative contribution of various sources from various regions is correct. Thus we use $\delta^{13}C$-CH_4 observations to help reduce uncertainties on source isotopic signatures. We test the ability of ship-based measurements to help constrain the isotopic signature of remote sources, such as wetland sources and oceanic emissions from the Laptev, East Siberian, and Chukchi Seas, dominant in the region explored during the campaign.

To do so, $\delta^{13}C$-CH_4 observations are implemented into a classical analytical Bayesian framework (Tarantola, 2005) using uncertainty and temporal correlations in signatures as detailed in Tab. 1. The inversion system optimizes source signatures from wetlands, solid fossil fuels, oil and gas, other anthropogenic sources, and a potential variety of marine sources (gas field leaks, decomposing hydrates, degrading permafrost, etc.) from the East Siberian Arctic Shelf (ESAS). Apart from ESAS, emissions are spatially differentiated into 24 geographical regions (see Figure 1). Contributions from different regions and

Table 1. Assumed isotopic signatures for the different components of CHIMERE forcings. The min-max range is centered around the prior signature. Prior signatures are selected from Sherwood et al. (2017) and Sapart et al. (2017).

Emission type	Prior signature (‰)	Min-Max range (‰)	Temporal correlation (days)
Wetlands	-65	25	30
Fossil solid	-55	25	30
Oil & gas	-42	15	30
Other anthropogenic	-60	10	30
ESAS	-55	25	10
Boundary concentrations (sides)	-47.5	2	30
Boundary concentrations (top)	-47.5	3	30

sectors are differentiated by computing so-called response functions by region, emission type and boundary side. That is to say, we carry out individual CHIMERE chemistry-transport simulations for every region, every type of emission and every side of the domain, all the other emissions and boundary conditions being switched off.

The simulated isotopic final composition is retrieved by scaling relative contributions according to assumed source signatures (or original average composition for boundary conditions). This allows us to easily compute and scale the simulated isotopic composition, but is a limiting factor as we do not account for the geographical variations of isotopic source signatures and the fact that the isotopic composition at the domain borders may vary independently from total CH_4.

3 Results and discussion

3.1 Forward modelling of total methane and isotopic ratio

Figure 2 shows observations of total CH_4 and of isotopic ratios as measured during the campaign and compared to simulations. The model CHIMERE reproduces well most of the variability in the total CH_4 signal. The average bias over the period is lower than 5 ppb with a correlation of 0.66 between observations and simulations on an hourly basis. Most peaks spanning more than one day are properly represented in the model, proving the capability of the model to reproduce the synoptic variability of the observations. Smaller peaks are missed by the model, in particular on Aug. 5, 12 and 15, indicating that some local sources are not included in the model, or are dispersed too quickly in the numerical realm. These could be local intense seeps met along the ship cruise, or shore wetlands not well represented with the model ORCHIDEE at $0.5°$ horizontal resolution. We do not investigate further missing emissions as most peaks are well explained by the model which we assume sufficient to carry out an inversion of isotopic signatures as described in Sect. 3.2.

When computing the intersect with the y-axis of the linear fit between δ^{13}C-CH_4 and total CH_4 (see Keeling plots in Supplementary material), the observed isotope ratios point to an average generic Arctic source of $-63.0‰$, consistent with dominant biogenic sources in Arctic regions. The model reproduces well this average signature at $-59.5‰$. Observations highlight a strong synoptic variability in isotopic ratios in the Arctic, with a standard deviation of $0.50‰$ and a range of $2‰$. Most of this is missed by the model (see Fig. 2, bottom panel). Simulated ratios with fixed (temporally and spatially) isotopic signatures for the emission sectors detailed in Sect. 2.3 barely exhibit any variations. The standard deviation is $0.22‰$ (resp. $0.12‰$ when removing the wetland event on August 21st), with a range of $1.5‰$ (resp. $0.5‰$). Considering the good fit of simulations to observations of total CH_4 , the missing variability indicates that the classical assumption of uniform signatures for given sectors and regions is not valid in the Arctic, consistent with Ganesan et al. (2018) and Fisher et al. (2011). Contributions to modelled concentrations from different regions of a given emission sector can change much more than the variability of total CH_4 as indicated in Fig. 2. For instance, on July 22nd, contributions from wetlands turn from a dominating Siberian influence to a North American one, causing a change of ~ 30 ppb in the signal. Differences in the average wetland source signatures between these two regions of $\sim 20‰$ (as suggested by Ganesan et al., 2018) would thus translate into $\sim 0.3‰$ in measured isotopic ratio, partly explaining the corresponding observed event.

More critical for the composition of air masses are the changes in hemispheric very large-scale contributions. As indicated by the blue shades in Fig. 2, depending on the dominant large scale transport patterns, contributions from the stratosphere and from the model lateral sides (located in the Tropics) can vary by more than 400 ppb within a few days. This corresponds to dominantly updraught or downdraught transport patterns, as illustrated by Fig. S2 in Supplement. These very strong variations in total CH_4 enhance the impact of uncertainties in the hemispheric vertical and horizontal distribution of isotopic ratios. First, tropical air masses are influenced by tropical wetlands and anthropogenic emissions, causing a spatial and temporal variability in tropical isotopic ratio of up to $1‰$, which is not accounted for in our CHIMERE set-up with fixed isotopic ratios at the simulation domain sides (see Sect.2.2). Second, the vertical profiles of isotopic ratios in the Arctic (see simulated example from the global transport model LMDZ in Fig. S3 in Supplement) are very steep. Such gradients are poorly represented in most

global models, due to issues in the representation of the vertical transport or to the insufficiently quantified fractionating OH and chlorine sinks in the stratosphere and upper troposphere. These two sources of uncertainties in chemistry-transport models

15 coupled with the strong real-world variations in stratospheric and tropospheric contributions could explain why the model does not reproduce the strong synoptic variability in δ^{13}C-CH$_4$ observed during the SWERUS-C3 campaign. In particular, for the above-mentioned event of July 22nd, contributions from the CHIMERE domain sides, vary by more than 300 ppb. Such a variability in CH$_4$ contributions, associated with differences of a few ‰ between the isotopic ratios of lower stratosphere airmasses and mid/low latitude air masses, could explain the observed event.

20 Thus, the first order variability of isotopic ratios is a balance between non-regional transport-related hemispheric features and regional contributions of wetland, ocean and anthropogenic emissions.
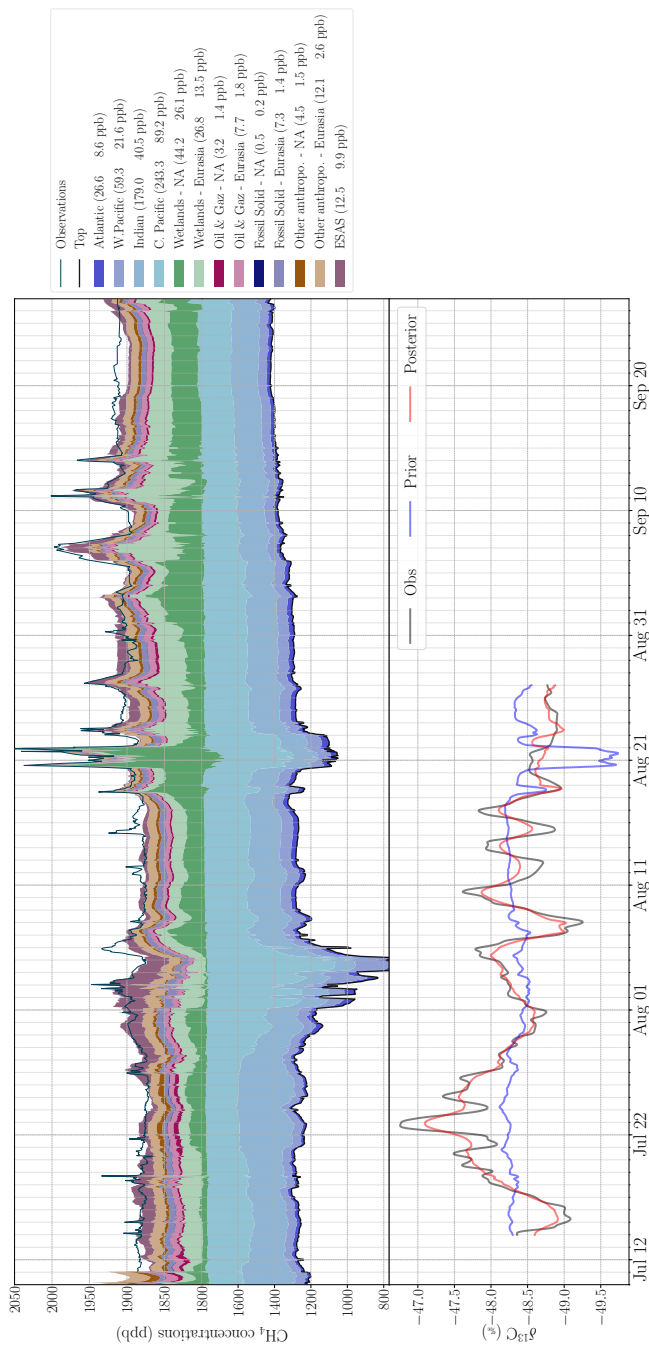
Figure 2. (top panel) Observed total CH$_4$ concentrations and simulated contributions to total CH$_4$ concentrations; only regions contributing more than 10 ppb on average are represented in the legend; the region ID and model side names are those of Fig. 1; light green areas depict Siberian wetlands, while dark green ones are North American wetlands. Shaded blue areas represent contributions from the sides of the CHIMERE simulation domain (see Fig. 1); orange shades represent minor anthropogenic contribution. So-called "top" line gives the simulated concentrations originating from the lower stratosphere (i.e., from the top of CHIMERE simulation domain). (bottom panel) Observed and simulated isotopic signatures before (prior) and after (posterior) inversion.
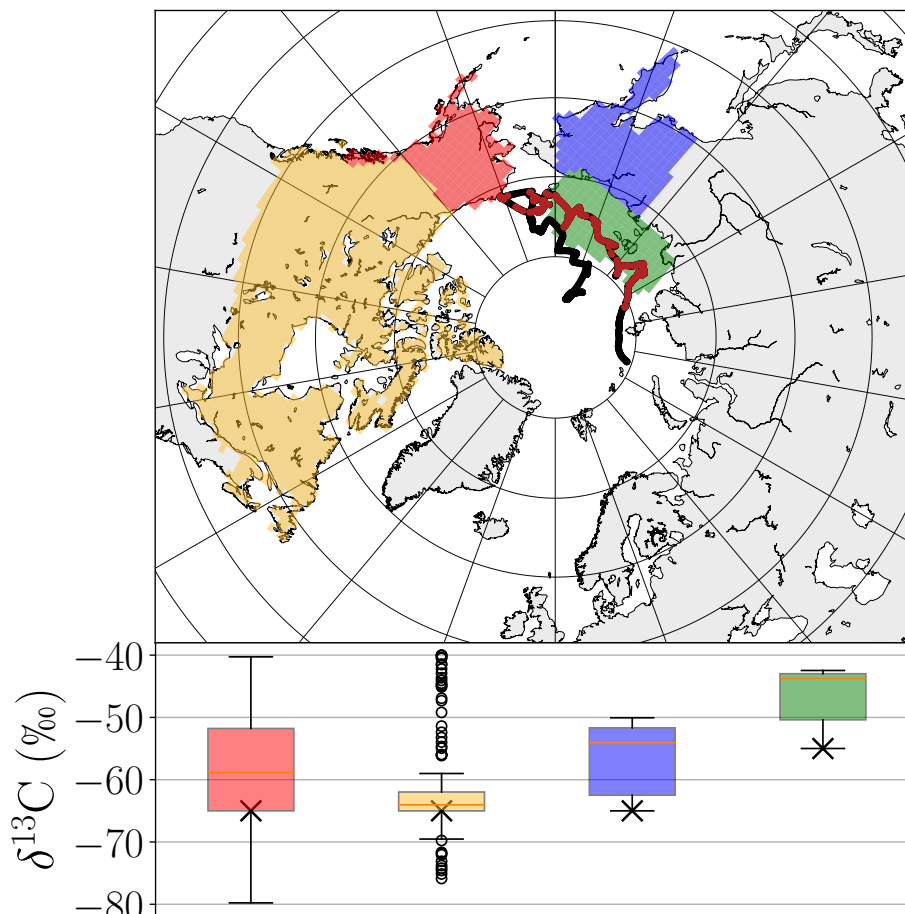
Figure 3. (top panel) Map of regions constrained by the observations (red points). (bottom panel) Range of posterior hourly signatures as deduced by the inversion for regions constrained by the observations. Prior signatures (black crosses) are those of Tab. 1. The total number of hours with isotopic data is 1057.

3.2 Optimisation of Arctic source signatures

Assuming that the mix of CH_4 sources is correct, we now attempt to separate hemispheric and regional contributions by optimizing source signatures for a set of geographical regions and different emission sectors in the Arctic as detailed in Sect. 2.3. Posterior ratios in Fig. 2 follow most of the variability in observations, indicating the inverse method does fit the observations

5 in a satisfying way. The rest of the signal is within the observation uncertainties of $0.1‰$.

  Figure 3 shows posterior signature distributions for the regions that are the most constrained by the observations, that is to say for which the uncertainty reduction is higher than 10% per day. Only the wetland emission sector is constrained for land regions in Fig. 3. Observational constraints on the other regions are too weak according to the inversion system to
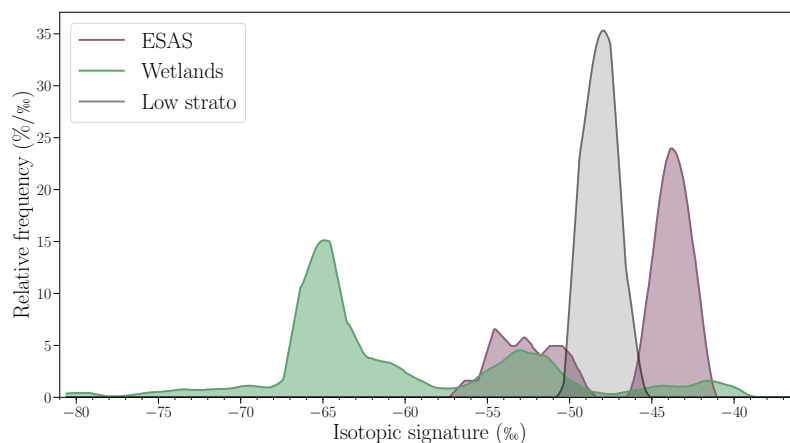
Figure 4. Posterior distribution of wetland and ESAS hourly signatures, as well as lower stratosphere isotopic ratio (i.e., model boundary conditions at the roof of the domain). Wetland regions are those of Fig. 3, i.e., the most constrained by observations in the inversion.

be shown here. Following this definition, only the roof boundary conditions (i.e., air masses from the lower stratosphere), ESAS emissions (i.e., emissions from the Laptev, East Siberian, and Chukchi Seas) and wetland regions on the shores of the Arctic ocean are reasonably constrained by the SWERUS-C3 ship-based campaign. Wetlands are suggested to have a heavier signature in Canada (median: $-64.0‰$) than in Eastern Siberia (median: $-54.0‰$), consistent with Ganesan et al. (2018) and

5 the compilation by Thornton et al. (2016b).

Fig. 4 summarizes the distributions of wetland and ESAS hourly signatures after optimization, as well a posterior signatures for airmasses coming from the lower stratosphere. The lower stratosphere signatures span in a short range of $-48.5/-46.5‰$. The atmospheric optimization suggests that the signatures of wetlands and ESAS span a very wide range of more than $10‰$. Wetland posterior distributions have three modes in the ranges $-70/-60‰$, $-57/-50‰$ and $-46/-39‰$. The two first

10 modes corresponds to wetlands in North America and Eastern Siberia respectively. The third mode is not consistent with any observed wetland signature to our knowledge; it is likely explained by the inversion system attributing part of the signal to thermogenic sources co-located with wetland emissions, as it is the case in both Siberia and Canada with extensive extraction of raw oil and gas.

Posterior ESAS signatures are mostly distributed in the range -48/-40‰ (median: $-43.7‰$), with a secondary mode in

15 the range -50/-58‰. This compares with previous studies and points towards a mix of different processes taking place in the Arctic shelf such as inputs from the sea bed (James et al., 2016; Berchet et al., 2016; Skorokhod et al., 2016; Pankratova et al., 2018). The lighter mode is dominated by thermogenic sources while the heavier mode could be explained by mixed biogenic and thermogenic sources, confirming that ESAS emissions, possibly including an hydrate contribution, are not as depleted as wetland sources (Cramer et al., 1999; Lorenson, 1999).

20 Overall, the approach developed here reveals that the spatial and temporal variations of isotopic source signatures must be accounted for in order to properly represent δ^{13}C-CH$_4$ observations. Such an approach does not allow us to reach definitive

conclusions when considering the spread of the inferred regional isotopic signatures. However, it is crucial to account for isotopic ratios to avoid misallocating methane flux variations in methane inversions. We also show that atmospheric δ^{13}C-CH$_4$ signals can be significant (larger than observation errors), indicating a good potential for the use of isotopic observations based on oceanic campaign to improve our knowledge of the Arctic methane cycle. Finally, the weight of the boundary conditions in

5   the signal points at necessary progress in global simulations (including fractionating chemical reactions in the stratosphere) of CH$_4$ isotopic ratios.

4   Conclusions

Observations of total methane and isotopic ratio were carried out in Summer 2014 in the Arctic Ocean during the SWERUS-C3 campaign onboard the Swedish icebreaker *Oden*. A unique continuous dataset of 45 days of isotopic ratio in the Arctic Ocean

10   is available from this campaign. Consistently with other campaigns in the region collecting flasks, the synoptic variability of isotopic ratios in the Arctic is very strong, spanning $\sim$ 2‰, largely above observation error. Using forward simulations, we confirmed that the assumption of uniform isotopic signature to represent emission sectors is invalid in the Arctic dominated by natural sources. We also exhibited the strong dependency of isotopic ratios to large-scale changes in air mass origin (lateral boundaries of our simulation domain, corresponding to mid-/low-latitude air masses; top boundaries corresponding to lower

15   stratosphere air masses). Based on a simplified inversion framework, the SWERUS-C3 data were used to infer isotopic source signatures of the Arctic regions and emission sectors. Wetland and oceanic ESAS source signatures were found to span a very wide range with a multimodal distribution for ESAS. The inversion also indicated that CH$_4$ emissions from ESAS are composed of a mixture of dominant thermogenic methane, complemented by some biogenic methane.

Overall, only a strong spatial and temporal variability in emission signatures and in stratospheric isotopic ratios can explain

20   the variability of observations. Therefore, our study points at necessary improvements in simulating the first-order transport and chemistry of methane and its isotopes to reproduce large scale hemispheric features, especially stratosphere to troposphere exchanges. This makes it necessary to improve i) the quality of continuous isotopic measurements to capture the synoptic signal with even higher confidence, ii) numerical chemistry-transport models, so that the uncertainties on the first-order processes are at least one order of magnitude smaller than the regional signal which is not the case today, and iii) the mapping of isotopic

25   emission signatures used as prior in inversions as initiated by Ganesan et al. (2018).

Author contribution

AB, TT and IP designed the simulation experiments. AB and TT developed the code and performed the CHIMERE numerical simulations. TH and JT run global simulations. PC and BT designed, carried out and provided observation data from the SWERUS-C3 campaign. PB, MS and JDP contributed to the scientific analysis of this work. AB prepared the manuscript with

30   contribution from all co-authors.

Acknowledgements. We thank the crew of I/B *Oden* who made the SWERUS-C3 expedition possible. SWERUS-C3 funding was provided by the Knut and Alice Wallenberg Foundation, Vetenskapsrådet (Swedish Research Council), Stockholm University, Swedish Polar Research Secretariat, and the Bolin Centre for Climate Research. δ^{13}C-CH$_4$ observations from SWERUS-C3 campaign will be posted to the Bolin Centre database, https://bolin.su.se/data/. This work has been supported by the Franco-Swedish IZOMET-FS "Distinguishing Arctic CH$_4$

5   sources to the atmosphere using inverse analysis of high-frequency CH$_4$, δ^{13}C-CH$_4$ and CH$_3$D measurements" project. The study extensively relies on the meteorological data provided by the ECMWF. Calculations were performed using the computing resources of LSCE, maintained by François Marabelle and the LSCE IT team.

References

Archer, D.: Methane hydrate stability and anthropogenic climate change, Biogeosciences, 4, 521–544, https://doi.org/https://doi.org/10.5194/bg-4-521-2007, https://www.biogeosciences.net/4/521/2007/, 2007.

Arora, V. K., Berntsen, T., Biastock, A., Bousquet, P., Bruhwiler, L., Bush, E., Chan, E., Christensen, T. R., Dlugokencky, E., Fisher, R. E., France, J., Gauss, M., H\"oglund-Isaksson, L., Houweling, S., Huissteden, K., and Janssens-Maenhout, G.: AMAP, 2015. AMAP Assessment 2015: Methane as an Arctic climate forcer, Tech. rep., Arctic Monitoring and Assessment Programme (AMAP), Oslo, Norway, https://www.amap.no/documents/doc/amap-assessment-2015-methane-as-an-arctic-climate-forcer/1285, 2015.

Arshinov, M. Y., Belan, B. D., Davydov, D. K., Inouye, G., Krasnov, O. A., Maksyutov, S., Machida, T., Fofonov, A. V., and Shimoyama, K.: Spatial and temporal variability of CO_2 and CH_4 concentrations in the surface atmospheric layer over West Siberia, Atmos Ocean Opt, 22, 84–93, https://doi.org/10.1134/S1024856009010126, http://link.springer.com/article/10.1134/S1024856009010126, 2009.

Berchet, A., Pison, I., Chevallier, F., Paris, J.-D., Bousquet, P., Bonne, J.-L., Arshinov, M. Y., Belan, B. D., Cressot, C., Davydov, D. K., Dlugokencky, E. J., Fofonov, A. V., Galanin, A., Lavrič, J., Machida, T., Parker, R., Sasakawa, M., Spahni, R., Stocker, B. D., and Winderlich, J.: Natural and anthropogenic methane fluxes in Eurasia: a meso-scale quantification by generalized atmospheric inversion, Biogeosciences Discuss., 11, 14 587–14 637, https://doi.org/10.5194/bgd-11-14587-2014, http://www.biogeosciences-discuss.net/11/14587/2014/, 2014.

Berchet, A., Bousquet, P., Pison, I., Locatelli, R., Chevallier, F., Paris, J.-D., Dlugokencky, E. J., Laurila, T., Hatakka, J., Viisanen, Y., Worthy, D. E. J., Nisbet, E., Fisher, R., France, J., Lowry, D., Ivakhov, V., and Hermansen, O.: Atmospheric constraints on the methane emissions from the East Siberian Shelf, Atmos. Chem. Phys., 16, 4147–4157, https://doi.org/10.5194/acp-16-4147-2016, http://www.atmos-chem-phys.net/16/4147/2016/, 2016.

Bohn, T. J., Melton, J. R., Ito, A., Kleinen, T., Spahni, R., Stocker, B. D., Zhang, B., Zhu, X., Schroeder, R., Glagolev, M. V., Maksyutov, S., Brovkin, V., Chen, G., Denisov, S. N., Eliseev, A. V., Gallego-Sala, A., McDonald, K. C., Rawlins, M., Riley, W. J., Subin, Z. M., Tian, H., Zhuang, Q., and Kaplan, J. O.: WETCHIMP-WSL: intercomparison of wetland methane emissions models over West Siberia, Biogeosciences, 12, 3321–3349, https://doi.org/10.5194/bg-12-3321-2015, http://www.biogeosciences.net/12/3321/2015/, 2015.

Charkin, A. N., Dudarev, O. V., Semiletov, I. P., Kruhmalev, A. V., Vonk, J. E., S\`anchez-Garc\'ia, L., Karlsson, E., and Gustafsson, \.: Seasonal and interannual variability of sedimentation and organic matter distribution in the Buor-Khaya Gulf: the primary recipient of input from Lena River and coastal erosion in the southeast Laptev Sea, Biogeosciences, 8, 2581–2594, https://doi.org/https://doi.org/10.5194/bg-8-2581-2011, https://www.biogeosciences.net/8/2581/2011/bg-8-2581-2011.html, 2011.

Craig, H.: Isotopic standards for carbon and oxygen and correction factors for mass-spectrometric analysis of carbon dioxide, Geochimica et Cosmochimica Acta, 12, 133–149, https://doi.org/10.1016/0016-7037(57)90024-8, http://www.sciencedirect.com/science/article/pii/0016703757900248, 1957.

Cramer, B., Poelchau, H. S., Gerling, P., Lopatin, N. V., and Littke, R.: Methane released from groundwater: the source of natural gas accumulations in northern West Siberia, Marine and Petroleum Geology, 16, 225–244, https://doi.org/10.1016/S0264-8172(98)00085-3, http://www.sciencedirect.com/science/article/pii/S0264817298000853, 1999.

Crippa, M., Janssens-Maenhout, G., Dentener, F., Guizzardi, D., Sindelarova, K., Muntean, M., Van Dingenen, R., and Granier, C.: Forty years of improvements in European air quality: regional policy-industry interactions with global impacts, Atmospheric Chemistry and Physics, 16, 3825–3841, https://doi.org/https://doi.org/10.5194/acp-16-3825-2016, https://www.atmos-chem-phys.net/16/3825/2016/, 2016.

Dlugokencky, E. J., Bruhwiler, L., White, J. W. C., Emmons, L. K., Novelli, P. C., Montzka, S. A., Masarie, K. A., Lang, P. M., Crotwell, A. M., Miller, J. B., and Gatti, L. V.: Observational constraints on recent increases in the atmospheric CH$_4$ burden, Geophys. Res. Lett., 36, L18 803, https://doi.org/10.1029/2009GL039780, http://onlinelibrary.wiley.com/doi/10.1029/2009GL039780/abstract, 2009.

Dlugokencky, E. J., Crotwell, A. M., Lang, P. M., and Masarie, K. A.: Atmospheric methane dry air mole Fractions from quasi-continuous
5   measurements at Barrow, Alaska and Mauna Loa, Hawaii, 1986-2013, ftp://ftp.cmdl.noaa.gov/ccg/ch4/in-situ/, 2014.

Dmitrenko, I. A., Kirillov, S. A., Tremblay, L. B., Kassens, H., Anisimov, O. A., Lavrov, S. A., Razumov, S. O., and Grigoriev, M. N.: Recent changes in shelf hydrography in the Siberian Arctic: Potential for subsea permafrost instability, Journal of Geophysical Research: Oceans, 116, https://doi.org/10.1029/2011JC007218, https://agupubs.onlinelibrary.wiley.com/doi/10.1029/2011JC007218, 2011.

Fisher, R. E., Sriskantharajah, S., Lowry, D., Lanoisellé, M., Fowler, C. M. R., James, R. H., Hermansen, O., Lund Myhre, C., Stohl, A.,
10   Greinert, J., Nisbet-Jones, P. B. R., Mienert, J., and Nisbet, E. G.: Arctic methane sources: Isotopic evidence for atmospheric inputs, Geophys. Res. Lett., 38, L21 803, https://doi.org/10.1029/2011GL049319, http://onlinelibrary.wiley.com/doi/10.1029/2011GL049319/abstract, 2011.

Fisher, R. E., France, J. L., Lowry, D., Lanoisellé, M., Brownlow, R., Pyle, J. A., Cain, M., Warwick, N., Skiba, U. M., Drewer, J., Dinsmore, K. J., Leeson, S. R., Bauguitte, S. J.-B., Wellpott, A., O'Shea, S. J., Allen, G., Gallagher, M. W., Pitt, J., Percival, C. J., Bower, K.,
15   George, C., Hayman, G. D., Aalto, T., Lohila, A., Aurela, M., Laurila, T., Crill, P. M., McCalley, C. K., and Nisbet, E. G.: Measurement of the 13C isotopic signature of methane emissions from northern European wetlands, Global Biogeochemical Cycles, 31, 605–623, https://doi.org/10.1002/2016GB005504, https://agupubs.onlinelibrary.wiley.com/doi/abs/10.1002/2016GB005504, 2017.

Ganesan, A. L., Stell, A. C., Gedney, N., Comyn-Platt, E., Hayman, G., Rigby, M., Poulter, B., and Hornibrook, E. R. C.: Spatially Resolved Isotopic Source Signatures of Wetland Methane Emissions, Geophysical Research Letters, 45, 3737–3745,
20   https://doi.org/10.1002/2018GL077536, https://agupubs.onlinelibrary.wiley.com/doi/abs/10.1002/2018GL077536, 2018.

James, R. H., Bousquet, P., Bussmann, I., Haeckel, M., Kipfer, R., Leifer, I., Niemann, H., Ostrovsky, I., Piskozub, J., Rehder, G., Treude, T., Vielstädte, L., and Greinert, J.: Effects of climate change on methane emissions from seafloor sediments in the Arctic Ocean: A review, Limnology and Oceanography, 61, S283–S299, https://doi.org/10.1002/lno.10307, https://aslopubs.onlinelibrary.wiley.com/doi/abs/10.1002/lno.10307, 2016.

25   Kirschke, S., Bousquet, P., Ciais, P., Saunois, M., Canadell, J. G., Dlugokencky, E. J., Bergamaschi, P., Bergmann, D., Blake, D. R., Bruhwiler, L., Cameron-Smith, P., Castaldi, S., Chevallier, F., Feng, L., Fraser, A., Heimann, M., Hodson, E. L., Houweling, S., Josse, B., Fraser, P. J., Krummel, P. B., Lamarque, J.-F., Langenfelds, R. L., Le Quéré, C., Naik, V., O'Doherty, S., Palmer, P. I., Pison, I., Plummer, D., Poulter, B., Prinn, R. G., Rigby, M., Ringeval, B., Santini, M., Schmidt, M., Shindell, D. T., Simpson, I. J., Spahni, R., Steele, L. P., Strode, S. A., Sudo, K., Szopa, S., van der Werf, G. R., Voulgarakis, A., van Weele, M., Weiss, R. F., Williams, J. E., and Zeng, G.: Three decades of
30   global methane sources and sinks, Nature Geosci, 6, 813–823, https://doi.org/10.1038/ngeo1955, http://www.nature.com/ngeo/journal/v6/n10/full/ngeo1955.html, 2013.

Lorenson, T.: Gas composition and isotopic geochemistry of cuttings, core, and gas hydrate from the JAPEX/JNOC/GSC Mallik 2L-38 gas hydrate research well, Bulletin of the Geological Survey of Canada, p. 21, http://pubs.er.usgs.gov/publication/70021662, 1999.

McCalley, C. K., Woodcroft, B. J., Hodgkins, S. B., Wehr, R. A., Kim, E.-H., Mondav, R., Crill, P. M., Chanton, J. P., Rich, V. I., Tyson,
35   G. W., and Saleska, S. R.: Methane dynamics regulated by microbial community response to permafrost thaw, Nature, 514, 478–481, https://doi.org/10.1038/nature13798, https://www.nature.com/articles/nature13798, 2014.

McGuire, A. D., Anderson, L. G., Christensen, T. R., Dallimore, S., Guo, L., Hayes, D. J., Heimann, M., Lorenson, T. D., Macdon-
ald, R. W., and Roulet, N.: Sensitivity of the carbon cycle in the Arctic to climate change, Ecological Monographs, 79, 523–555,
https://doi.org/10.1890/08-2025.1, http://www.esajournals.org/doi/abs/10.1890/08-2025.1, 2009.

Menut, L., Bessagnet, B., Khvorostyanov, D., Beekmann, M., Blond, N., Colette, A., Coll, I., Curci, G., Foret, G., Hodzic, A., Mailler, S.,
Meleux, F., Monge, J.-L., Pison, I., Siour, G., Turquety, S., Valari, M., Vautard, R., and Vivanco, M. G.: CHIMERE 2013: a model for
regional atmospheric composition modelling, Geosci. Model Dev., 6, 981–1028, https://doi.org/10.5194/gmd-6-981-2013, http://www.
geosci-model-dev.net/6/981/2013/, 2013.

Nisbet, E. G., Dlugokencky, E. J., Manning, M. R., Lowry, D., Fisher, R. E., France, J. L., Michel, S. E., Miller, J. B., White, J. W. C.,
Vaughn, B., Bousquet, P., Pyle, J. A., Warwick, N. J., Cain, M., Brownlow, R., Zazzeri, G., Lanoisellé, M., Manning, A. C., Gloor, E.,
Worthy, D. E. J., Brunke, E.-G., Labuschagne, C., Wolff, E. W., and Ganesan, A. L.: Rising atmospheric methane: 2007–2014 growth
and isotopic shift, Global Biogeochemical Cycles, 30, 1356–1370, https://doi.org/10.1002/2016GB005406, https://agupubs.onlinelibrary.
wiley.com/doi/abs/10.1002/2016GB005406, 2016.

Nisbet, E. G., Manning, M. R., Dlugokencky, E. J., Fisher, R. E., Lowry, D., Michel, S. E., Myhre, C. L., Platt, S. M., Allen, G., Bousquet,
P., Brownlow, R., Cain, M., France, J. L., Hermansen, O., Hossaini, R., Jones, A. E., Levin, I., Manning, A. C., Myhre, G., Pyle, J. A.,
Vaughn, B. H., Warwick, N. J., and White, J. W. C.: Very Strong Atmospheric Methane Growth in the 4 Years 2014–2017: Implications for
the Paris Agreement, Global Biogeochemical Cycles, 33, 318–342, https://doi.org/10.1029/2018GB006009, https://agupubs.onlinelibrary.
wiley.com/doi/abs/10.1029/2018GB006009, 2019.

Pankratova, N., Skorokhod, A., Belikov, I., Elansky, N., Rakitin, V., Shtabkin, Y., and Berezina, E.: EVIDENCE OF ATMOSPHERIC
RESPONSE TO METHANE EMISSIONS FROM THE EAST SIBERIAN ARCTIC SHELF, https://ges.rgo.ru/jour/article/view/383,
2018.

Pankratova, N., Belikov, I., Skorokhod, A., Belousov, V., Artamonov, A., Repina, I., and Shishov, E.: Measurements and data processing
of atmospheric CO$_2$, CH$_4$, H$_2$O and δ^{13}C-CH$_4$ mixing ratio during the ship campaign in the East Arctic and
the Far East seas in autumn 2016, IOP Conf. Ser.: Earth Environ. Sci., 231, 012 041, https://doi.org/10.1088/1755-1315/231/1/012041,
https://doi.org/10.1088%2F1755-1315%2F231%2F1%2F012041, 2019.

Paris, J. D., Ciais, P., Nédélec, P., Stohl, A., Belan, B. D., Arshinov, M. Y., Carouge, C., Golitsyn, G. S., and Granberg, I. G.: New insights
on the chemical composition of the Siberian air shed from the YAK-AEROSIB aircraft campaigns, B. Am. Meteorol. Soc., 91, 625–641,
http://zardoz.nilu.no/~andreas/publications/168.pdf, 2010.

Ringeval, B., de Noblet-Ducoudré, N., Ciais, P., Bousquet, P., Prigent, C., Papa, F., and Rossow, W. B.: An attempt to quantify the im-
pact of changes in wetland extent on methane emissions on the seasonal and interannual time scales, Global Biogeochemical Cy-
cles, 24, https://doi.org/10.1029/2008GB003354, http://onlinelibrary.wiley.com.biblioplanets.gate.inist.fr/doi/10.1029/2008GB003354/
abstract, 2010.

Ruppel, C. D. and Kessler, J. D.: The interaction of climate change and methane hydrates, Reviews of Geophysics, 55, 126–168,
https://doi.org/10.1002/2016RG000534, https://agupubs.onlinelibrary.wiley.com/doi/10.1002/2016RG000534, 2017.

Sapart, C. J., Shakhova, N., Semiletov, I., Jansen, J., Szidat, S., Kosmach, D., Dudarev, O., Veen, C. v. d., Egger, M., Sergienko, V., Salyuk, A.,
Tumskoy, V., Tison, J.-L., and Röckmann, T.: The origin of methane in the East Siberian Arctic Shelf unraveled with triple isotope analysis,
Biogeosciences, 14, 2283–2292, https://doi.org/https://doi.org/10.5194/bg-14-2283-2017, https://www.biogeosciences.net/14/2283/2017/,
2017.

Sasakawa, M., Shimoyama, K., Machida, T., Tsuda, N., Suto, H., Arshinov, M., Davydov, D., Fofonov, A., Krasnov, O., Saeki, T., Koyama, Y., and Maksyutov, S.: Continuous measurements of methane from a tower network over Siberia, Tellus B, 62, 403–416, https://doi.org/10.1111/j.1600-0889.2010.00494.x, http://onlinelibrary.wiley.com/doi/10.1111/j.1600-0889.2010.00494.x/abstract, 2010.

Saunois, M., Bousquet, P., Poulter, B., Peregon, A., Ciais, P., Canadell, J. G., Dlugokencky, E. J., Etiope, G., Bastviken, D., Houweling, S.,

5 Janssens-Maenhout, G., Tubiello, F. N., Castaldi, S., Jackson, R. B., Alexe, M., Arora, V. K., Beerling, D. J., Bergamaschi, P., Blake, D. R., Brailsford, G., Brovkin, V., Bruhwiler, L., Crevoisier, C., Crill, P., Covey, K., Curry, C., Frankenberg, C., Gedney, N., Höglund-Isaksson, L., Ishizawa, M., Ito, A., Joos, F., Kim, H.-S., Kleinen, T., Krummel, P., Lamarque, J.-F., Langenfelds, R., Locatelli, R., Machida, T., Maksyutov, S., McDonald, K. C., Marshall, J., Melton, J. R., Morino, I., Naik, V., O'Doherty, S., Parmentier, F.-J. W., Patra, P. K., Peng, C., Peng, S., Peters, G. P., Pison, I., Prigent, C., Prinn, R., Ramonet, M., Riley, W. J., Saito, M., Santini, M., Schroeder, R., Simpson, I. J.,

10 Spahni, R., Steele, P., Takizawa, A., Thornton, B. F., Tian, H., Tohjima, Y., Viovy, N., Voulgarakis, A., Weele, M. v., Werf, G. R. v. d., Weiss, R., Wiedinmyer, C., Wilton, D. J., Wiltshire, A., Worthy, D., Wunch, D., Xu, X., Yoshida, Y., Zhang, B., Zhang, Z., and Zhu, Q.: The global methane budget 2000–2012, Earth System Science Data, 8, 697–751, https://doi.org/https://doi.org/10.5194/essd-8-697-2016, https://www.earth-syst-sci-data.net/8/697/2016/, 2016.

Saunois, M., Bousquet, P., Poulter, B., Peregon, A., Ciais, P., Canadell, J. G., Dlugokencky, E. J., Etiope, G., Bastviken, D., Houweling, S.,

15 Janssens-Maenhout, G., Tubiello, F. N., Castaldi, S., Jackson, R. B., Alexe, M., Arora, V. K., Beerling, D. J., Bergamaschi, P., Blake, D. R., Brailsford, G., Bruhwiler, L., Crevoisier, C., Crill, P., Covey, K., Frankenberg, C., Gedney, N., Höglund-Isaksson, L., Ishizawa, M., Ito, A., Joos, F., Kim, H.-S., Kleinen, T., Krummel, P., Lamarque, J.-F., Langenfelds, R., Locatelli, R., Machida, T., Maksyutov, S., Melton, J. R., Morino, I., Naik, V., O'Doherty, S., Parmentier, F.-J. W., Patra, P. K., Peng, C., Peng, S., Peters, G. P., Pison, I., Prinn, R., Ramonet, M., Riley, W. J., Saito, M., Santini, M., Schroeder, R., Simpson, I. J., Spahni, R., Takizawa, A., Thornton, B. F., Tian, H., Tohjima, Y.,

20 Viovy, N., Voulgarakis, A., Weiss, R., Wilton, D. J., Wiltshire, A., Worthy, D., Wunch, D., Xu, X., Yoshida, Y., Zhang, B., Zhang, Z., and Zhu, Q.: Variability and quasi-decadal changes in the methane budget over the period 2000–2012, Atmospheric Chemistry and Physics, 17, 11 135–11 161, https://doi.org/https://doi.org/10.5194/acp-17-11135-2017, https://www.atmos-chem-phys.net/17/11135/2017/, 2017.

Sherwood, O. A., Schwietzke, S., Arling, V. A., and Etiope, G.: Global Inventory of Gas Geochemistry Data from Fossil Fuel, Microbial and Burning Sources, version 2017, Earth System Science Data, 9, 639–656, https://doi.org/https://doi.org/10.5194/essd-9-639-2017,

25 https://www.earth-syst-sci-data.net/9/639/2017/, 2017.

Skorokhod, A. I., Pankratova, N. V., Belikov, I. B., Thompson, R. L., Novigatsky, A. N., and Golitsyn, G. S.: Observations of atmospheric methane and its stable isotope ratio (δ^{13}C) over the Russian Arctic seas from ship cruises in the summer and autumn of 2015, Dokl. Earth Sc., 470, 1081–1085, https://doi.org/10.1134/S1028334X16100160, https://doi.org/10.1134/S1028334X16100160, 2016.

Tan, Z., Zhuang, Q., Henze, D. K., Frankenberg, C., Dlugokencky, E., Sweeney, C., Turner, A. J., Sasakawa, M., and Machida, T.: In-

30 verse modeling of pan-Arctic methane emissions at high spatial resolution: what can we learn from assimilating satellite retrievals and using different process-based wetland and lake biogeochemical models?, Atmospheric Chemistry and Physics, 16, 12 649–12 666, https://doi.org/https://doi.org/10.5194/acp-16-12649-2016, https://www.atmos-chem-phys.net/16/12649/2016/, 2016.

Tarantola, A.: Inverse problem theory and methods for model parameter estimation: SIAM, Society for Industrial and Applied Mathematics, 3600, 19 104–2688, 2005.

35 Thompson, R. L., Sasakawa, M., Machida, T., Aalto, T., Worthy, D., Lavric, J. V., Lund Myhre, C., and Stohl, A.: Methane fluxes in the high northern latitudes for 2005–2013 estimated using a Bayesian atmospheric inversion, Atmos. Chem. Phys., 17, 3553–3572, https://doi.org/10.5194/acp-17-3553-2017, http://www.atmos-chem-phys.net/17/3553/2017/, 2017.

Thornton, B. F., Geibel, M. C., Crill, P. M., Humborg, C., and Mörth, C.-M.: Methane fluxes from the sea to the atmosphere across the Siberian shelf seas, Geophys. Res. Lett., 43, 2016GL068 977, https://doi.org/10.1002/2016GL068977, http://onlinelibrary.wiley.com/doi/10.1002/2016GL068977/abstract, 2016a.

Thornton, B. F., Wik, M., and Crill, P. M.: Double-counting challenges the accuracy of high-latitude methane inventories, Geophys. Res. Lett.,
5 p. 2016GL071772, https://doi.org/10.1002/2016GL071772, http://onlinelibrary.wiley.com/doi/10.1002/2016GL071772/abstract, 2016b.

Turner, A. J., Frankenberg, C., and Kort, E. A.: Interpreting contemporary trends in atmospheric methane, PNAS, 116, 2805–2813, https://doi.org/10.1073/pnas.1814297116, https://www.pnas.org/content/116/8/2805, 2019.

Warwick, N. J., Cain, M. L., Fisher, R., France, J. L., Lowry, D., Michel, S. E., Nisbet, E. G., Vaughn, B. H., White, J. W. C., and Pyle, J. A.: Using δ^{13}C-CH$_4$ and δD-CH$_4$ to constrain Arctic methane emissions, Atmos. Chem. Phys., 16, 14 891–14 908,
10 https://doi.org/10.5194/acp-16-14891-2016, http://www.atmos-chem-phys.net/16/14891/2016/, 2016.

Xiong, X., Barnet, C., Maddy, E., Sweeney, C., Liu, X., Zhou, L., and Goldberg, M.: Characterization and validation of methane products from the Atmospheric Infrared Sounder (AIRS), Journal of Geophysical Research: Biogeosciences, 113, https://doi.org/10.1029/2007JG000500, https://agupubs.onlinelibrary.wiley.com/doi/full/10.1029/2007JG000500, 2008.

Yu, J., Xie, Z., Sun, L., Kang, H., He, P., and Xing, G.: δ^{13}C-CH4 reveals CH4 variations over oceans from mid-latitudes to the Arctic,
15 Scientific Reports, 5, 13 760, https://doi.org/10.1038/srep13760, https://www.nature.com/articles/srep13760, 2015.